Artificial resonant crystals for hydroelastic waves

Supplementary Information

L. Domino, M. Fermigier, and A. Eddi

Laboratoire de Physique et Mécanique des Milieux Hétérogènes (PMMH), UMR CNRS 7636 ; ESPCI, Paris, France

I. HYDROELASTIC WAVES

To understand wave propagation at the surface of water covered with an elastic membrane one needs to study the coupling between the deformation of the membrane and the fluid motion. This calculation has been detailed in previous works [1–3], and we only show here a condensed version of it. The thin membrane obeys the Föppl-Von Kàrmàn equations

$$\begin{aligned} D\Delta^2\zeta - e\frac{\partial}{\partial x_\beta}\left(\sigma_{\alpha,\beta}\frac{\partial\zeta}{\partial x_\alpha}\right) &= P \\ \frac{\partial\sigma_{\alpha,\beta}}{\partial x_\beta} &= 0, \end{aligned} \tag{1}$$

where ζ is the wave amplitude, $D = \frac{Ee^3}{12(1-\nu^2)}$ is the flexural modulus of the membrane, α and β are the two main directions, $\sigma_{\alpha,\beta}$ is the stress along x_α applied to the surface orthogonal to x_β and P is the external pressure applied. In the liquid, neglecting viscosity and assuming that the flow in incompressible and irrotational, we can use the Bernoulli equation

$$\rho\frac{\partial\phi}{\partial t} + \rho\frac{\mathbf{v}^2}{2} + P + \rho g z = C, \tag{2}$$

where ϕ is the velocity potential, P is the pressure and C is an arbitrary constant. Because of continuity of stresses at the water-membrane interface, the two pressure terms in eq. 1 and eq. 2 are equal. We can also simplify both expression using $\zeta \ll e$ (the amplitude of the waves is small compared to the thickness of the membrane) and $\zeta \ll \lambda$ (small slopes). This leads to the follloxing dispersion relation :

$$\omega^2 = \frac{Dk^5/\rho + Tk^3/\rho + gk}{ek\rho/\rho_p + \coth kH}. \tag{3}$$

We plot in figure S1 this dispersion relation, for thicknesses $t = 100$ μm, 200 μm, 500 μm and 800 μm (solid lines). For $\rho \sim \rho_p$ and at high frequency / low wavelength it can be simplified as $\omega^2 = Dk^5/\rho$, and we show this approximated dispersion relation as dashed lines in S1.

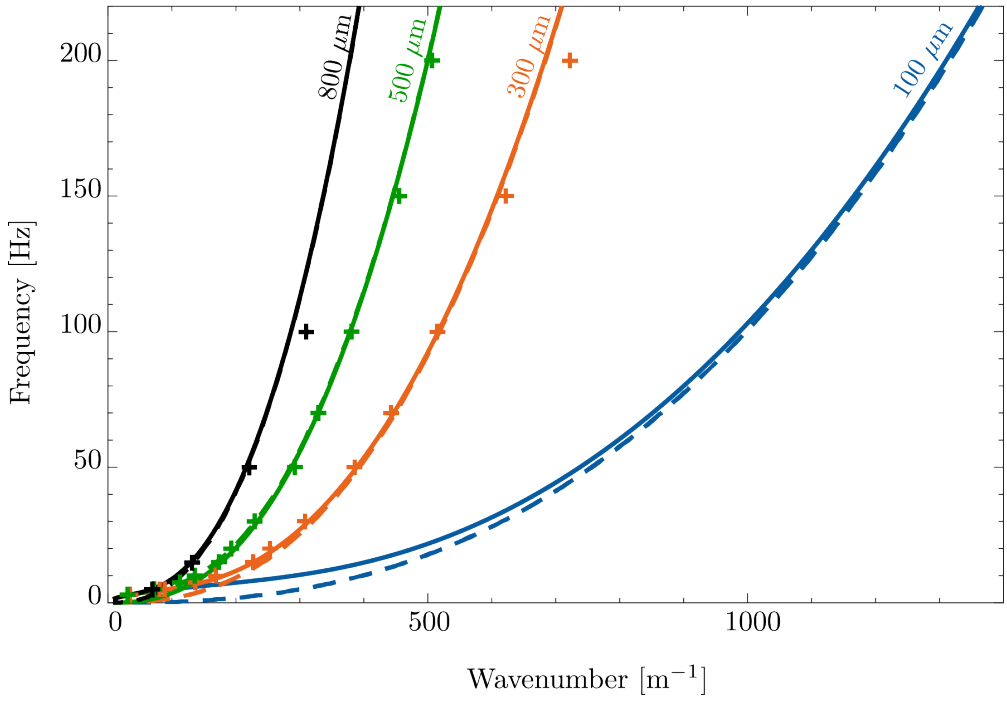

FIG. S1. (a) Dispersion relation for e = 100 μm, 300 μm, 500 μm and 800 μm, E = 1.6 MPa, $\rho = 965kg/m^3$. The thickness is increasing from right to left, and solid lines correspond to equation 3 while dashed lines is its simplified version $\omega^2 = Dk^5/\rho$. The data points (+) are taken from [3].

II. SCHLIEREN IMAGING TECHNIQUE

We use state-of-the-art techniques to measure the waves that propagate at the surface of water covered with an elastic membrane. We use a known pattern below the tank (either a random dot pattern for [4] or a checkerboard pattern for [5]), and we take images from the top. The pattern appears distorted due to refraction at the water-air interface (or more accurately the polymer-air interface, but here the elastic membrane is thin enough to be neglected for the refraction). We use an image taken when the surface is flat as a reference (fig. S2(a)) and compare it to a deformed image (fig. S2(c)) [6]. To compute the apparent displacement of the pattern we use the spatial Fourier spectra of the 2 images (fig. S2(b) and (d)) and extract the quantitative map of apparent deformation of the pattern. From this, and using ray optics theory, one can reconstruct the height profile of the wave, shown in fig. S2(e). With our experimental setup, we could measure wave amplitudes with a resolution of less than 1 μm. Supplementary Video 1 shows an animated version of fig. S2, with the raw images, their corresponding spectra and the reconstructed height field.

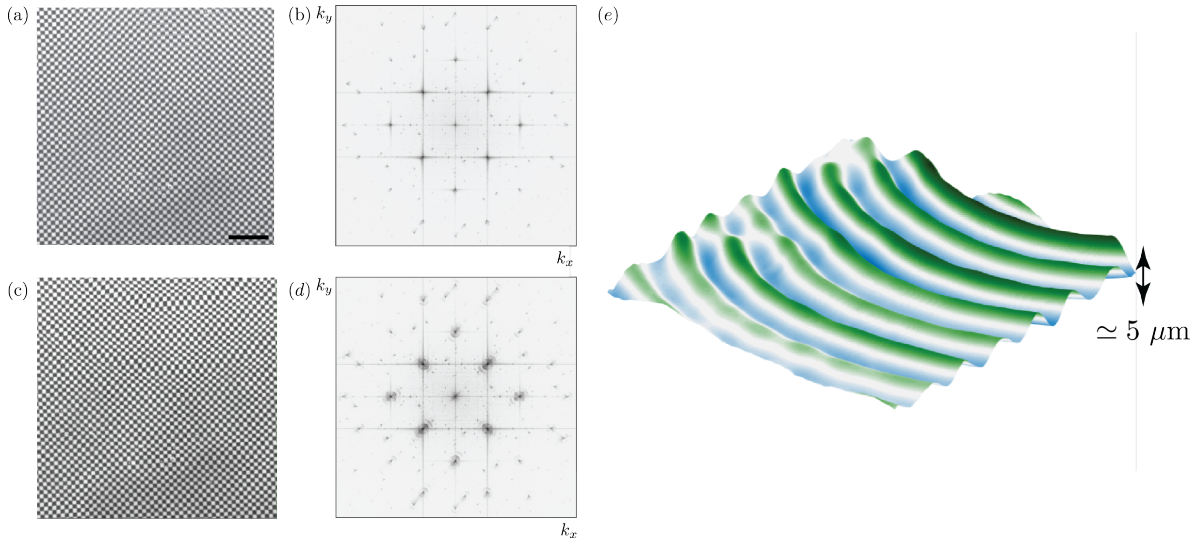

FIG. S2. (a) Reference image. The scale bar represents 2 cm. (b) Fourier spectrum of (a). (c) Deformed image. (d) Fourier spectrum of (c). (e) Reconstructed height profile.

III. CRYSTAL OF SCATTERERS : PILLARS

The first experiment we carried out was to glue on the floating membrane thick cylinders cut out in a thick polymer sheet. The thickness difference between the sheet and the pillars induces an index contrast, which should in turn introduce partial reflection of the waves. The cylinders are 4 mm in diameter and 1 mm high, and they are placed on the membrane according to a square lattice with spacing 1 cm (chosen to allow for a Bragg gap within our measuring range). We use 10 $\times$ 20 cylinders, placed on the 300 μm thick membrane. A picture of the obtained lattice is shown in fig. S3

We send a plane wave through the crystal along one of its main direction (x, see sketch in S3(b)), and we measure the wave field inside the crystal, using the method presented earlier. We use frequency sweeps between 20 Hz and 150 Hz, that we subsequently filter using FFT. This allows us to isolate for each forcing frequency the spatial 2D spectrum of the wave.

As the crystal is only probed in the x direction we keep the wavenumbers in the direction in the spectra, and stack them as a function of the frequency, to obtain the band structure represented in figure S3(d). As expected, it corresponds to the dispersion relation of hydroelastic waves in the homogeneous material (outside the crystal), folded with the symmetry of the crystal, *i.e.* on $k_x = \pm n2\pi/a$, where n is an integer [7]. To highlight this, we add the theoretical dispersion relation calculated for an homogeneous material, plus its trans-

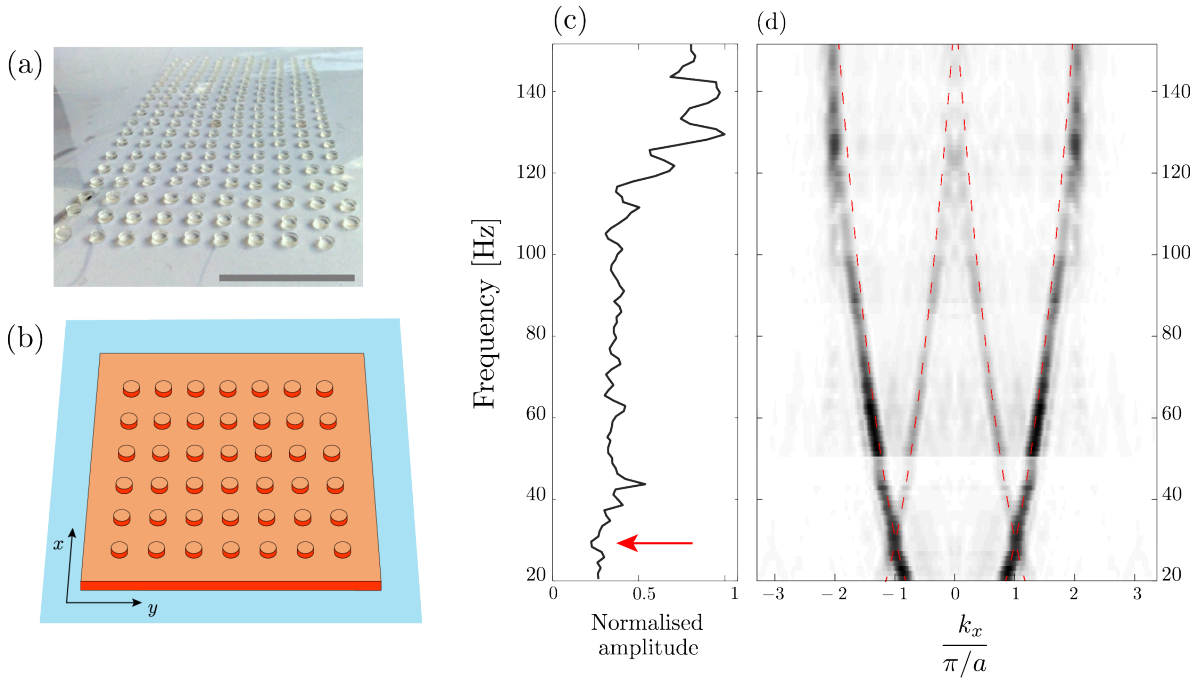

FIG. S3. (a) Square crystal made of cylinders of polymer at the surface of a membrane. The cylinders are 4 mm in diameter and 1 cm apart. The scale bar represents 5 cm. (b) Sketch of the experiement. (c) Average amplitude measured in the crystal as a function of the forcing frequency. (d) Dispersion relation measured along the x direction. Information is represented in grayscale and in a log scale. Red dashed curve : theoretical dispersion relation, folded with the symmetry of the crystal $k_x = \pm 2\pi/a$.

lated version centered on the wavenumber $k_x = \pm 2\pi/a$ (dashed red line in S3(d)). These symmetrised curves describe our results very well, and we note that two bands intersect at the edge of the First Brillouin zone ($k_x = \pi/a$). Of course, bands do not interesect in a real crystal, and we should observe a bandgap. There is no clear bandgap in this experiment, even when we plot the averaged wave amplitude as a function of the frequency (fig. S3(c)). Indeed, we should see a drop in amplitude around 28 Hz, which corresponds to the edge of the Brillouin zone, *i.e.* the intersection between two curves. This first Bragg bandgap is very narrow, with a very weak amplitude drop. This means that the pillars we use interact very little with the incident wave, and don't scatter much energy. The holes presented in the body text are better scatterers (as well as having resonances), which is why those crystals exhibit bigger Bragg bandgaps (see for instance figure 3c in the body text).

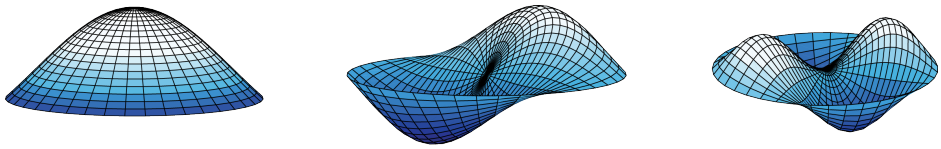

FIG. S4. (a)

IV. MODES OF CIRCULAR CAVITY

The family of solutions to the wave equation $\frac{\partial^2 u}{\partial t^2} = v_\varphi^2 \Delta u$ (where u is the amplitude of the wave, *i.e.* here it is the surface height) in a circular domain are the Bessel functions. Here we approximate the boundary condition to that of Dirichlet, so that $u = 0$ at the edge of the cavity $r = R$. In practice, the soft membrane deforms as the wave propagates, and the contact line is pinned at different height at the edge of the membrane ; both these effects modify the actual boundary condition. We discard the Bessel function of the second kind part of the solution as it diverges in $r = 0$. Denoting α_{mn} the n-th root of the Bessel function of the first kind J_m, the oscillating solution reads :

$$u(r, \theta, t) = A_2 J_m \left(\frac{\alpha_{mn}}{R} r \right) . \left(A_1 \cos m\theta + B_1 \sin m\theta \right) . A e^{i \frac{v_\varphi \alpha_{mn} t}{R}} . \tag{4}$$

This is a superposition of the eigenmodes mn of a Bessel function (the first three are shown in 4) that oscillates at a frequency $\omega = \frac{v_\varphi \alpha_{mn}}{R}$, where v_φ is the phase velocity of the gravity capillary waves. The first 9 values of α_{mn} are shown in the table below.

	m = 0	**m = 1**	**m = 2**
$n = 1$	$\alpha_{01} = 2.40$	$\alpha_{11} = 3.83$	$\alpha_{21} = 5.14$
$n = 2$	$\alpha_{02} = 5.52$	$\alpha_{12} = 7.02$	$\alpha_{22} = 8.42$
$n = 3$	$\alpha_{03} = 8.65$	$\alpha_{13} = 10.17$	$\alpha_{23} = 11.62$

TABLE S1. Values of the first 9 roots α_{mn} of J_m

To determine the oscillating frequency in our case, we use the dispersion relation of gravity-capillary waves $\omega^2 = \frac{\sigma}{\rho} k^3 + gk$ with the approximated value $\sigma \sim 50\ mN/m$. The three lowest frequencies for cavities of diameter 3 mm, 4 mm and 10 mm are shown in table S2.

	Mode 01	**Mode 11**	**Mode 21**
$\varnothing = 3\ mm$	75 Hz	147 Hz	227 Hz
$\varnothing = 4\ mm$	50 Hz	97 Hz	149 Hz
$\varnothing = 10\ mm$	16 Hz	28 Hz	40 Hz

TABLE S2. First three eigenfrequencies for three cavity diameters, calculated for a free surface, *ie.* using the gravity-capillary waves dispersion relation.

V. CALCULATION OF BAND STRUCTURES

The theoretical approach developped here is extensively inspired from previous work in acoustics [8–11], which adapted concepts of Fano resonance and optical multiple scattering theory to classical waves.

We model the response of a point resonator with eigenfrequency $f_0 = \omega_0/2\pi$ with the Lorentzian function [10, 12]

$$A(\omega) = \frac{2j\omega/c}{1 + 2jQ(1 - \omega/\omega_0)}, \tag{5}$$

where c is the wave velocity, here that of hydroelastic waves calculated with the equation 3, and Q is the quality factor of the resonator, that corresponds to its bandwidth (the higher the coupling between the resonator and the incident wave is, the lower the quality factor is). As expected from a resonance, this function $A(\omega)$ corresponds to a peak in the amplitude of the wave at $f = f_0$ and a phase jump of π. Note that this is an approximation as our resonators have a finite size.

To describe the interaction between a single point resonator and an incident wave, one can adapt the theory of Fano resonance to classical waves. This theory is relevant here as we are studying the interaction between two waves, one being highly localised and with discrete energy levels (*i.e.* the resonance), and the other being non-localised (*i.e.* the incident wave). The basic principle of the type of resonance is shown in figure S5(a) : the incident wave (in black) and the wave emitted by the resonator (in blue) interfere to give the transmitted wave (in green). This transmitted wave T is the sum between the incident wave and the emitted wave t, the amplitude and phase of the latter is shown in figure S5(b) : we recover

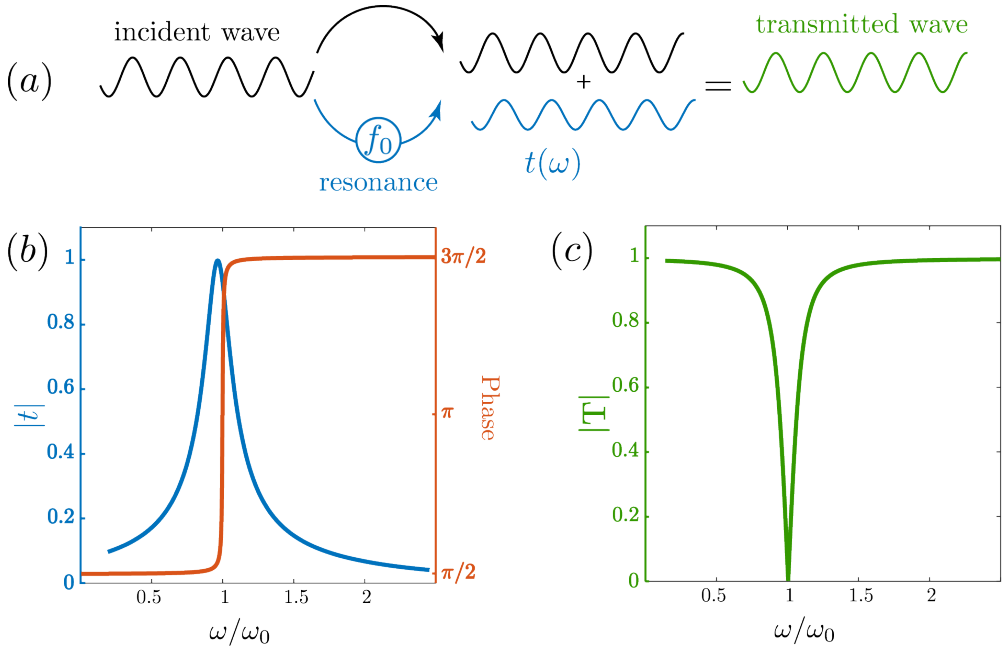

FIG. S5. (a) Sketch (b) Response t (c) Transmitted T

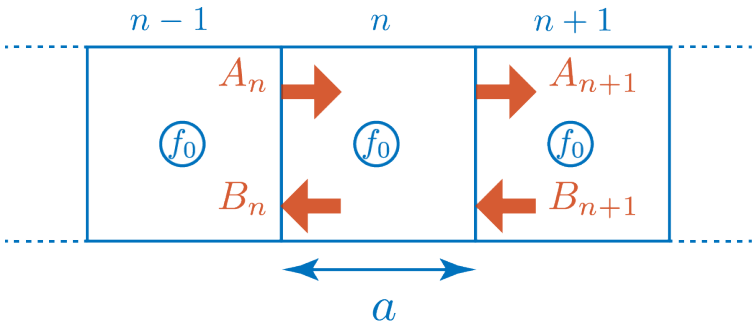

FIG. S6. Sketch showing the n-th unit cell of length a and the reflexion and transmission coefficients A_n, B_n, A_{n+1} and B_{n+1}

the Lorentz-like response for the amplitude and the π phase jump. The amplitude of the resulting transmitted wave T is shown in figure S5(c) : at the resonance, most of the incident energy is localised on the resonator.

We approximate the frequency response of the hole as the sum of individual resonators, assuming that its resonance frequencies are sufficiently apart. It yields

$$t(\omega) = t_{\omega_0}(\omega) + t_{\omega_1}(\omega) + t_{\omega_2}(\omega) + ..., \tag{6}$$

where $\omega_{0,1,2,...}$ are the successive resonance frequencies.

Now that we have a way to model the resonator, we can study the behavior of an organised lattice of them. We model the response of a 1D infinite lattice of resonators using the transfer matrix formalism. The distance between the resonators is the lattice constant a, and we define the unit cell of length a, centered on each resonator. This arrangement is schematically shown in figure S6. Our goal here is to express the transfer matrix M that links $A_n,\ B_n,\ A_{n+1}$ and B_{n+1} (shown in fig. S6) according to

$$\begin{pmatrix} A_{n+1} \\ B_{n+1} \end{pmatrix} = M \begin{pmatrix} A_n \\ B_n \end{pmatrix}.$$

The matrix M can be calculated from the resonator response in transmission T and in reflection R, and from the wave properties, namely the wave velocity c. Taking into account the phase shift $\frac{\omega}{c}a$ due to the propagation on a distance a and energy conservation, we find that the transfer matrix M writes

$$M = \begin{pmatrix} \frac{1}{T*}e^{j\frac{\omega}{c}a} & -\frac{R*}{T*} \\ -\frac{R}{T} & \frac{1}{T}e^{j\frac{\omega}{c}a} \end{pmatrix},$$

where '*' denotes the complex conjugate. In a periodic material, the solution to the wave equation are Bloch waves, which means that M must satisfy $\det(M - e^{jka}I) = 0$. This leads to the following dispersion relation :

$$\cos ka = Re\left(\frac{1}{T}e^{-j\frac{\omega}{c}a}\right). \tag{7}$$

We readily see that both resonance and periodicity effects are taken into account, and we can use the expression for T we establish earlier to calculate this dispersion relation numerically. Using this equation, we can predict the band structure of a resonant crystal, knowing the lattice constant a and the characteristics of the resonators.

Note that here we need to include dispersion, which we do by using the hydroelastic wave velocity $c = \frac{\omega}{k}$ calculated with eq.(3). In addition, we can't predict the exact resonance frequencies and bandwidths of the cavities, and our measurements only give qualitative

agreement with our observations, so that ω_0 and Q have to be adjustable parameters in our model. We considered the 3 lattices presented in figure **??**, for which we used the values for ω_0 and for Q detailed in the caption of figure 4.

VI. APPARENT REFRACTION IN A CRYSTAL

We probe the refraction of a plane wave at the interface between an homogeneous medium and a lattice made of holes of diameter 4 mm and with a lattice constant $a = 1$ cm for a non-zero incidence angle [fig. S7(a)]. Using a spatial Fourier transform, we extract the isofrequency spectrum corresponding to wave propagation in the lattice [figure S7(b)].

We observe several peaks with different wavenumbers k_x and k_y. We superimpose to this spatial spectrum circles whose radius matches the hydroelastic wavenumber at the forcing frequency. Those circles (shown in white in fig. **??**(b)) are centered on the points of the reciprocal lattice located in the first and second Brillouin zone. We denote with blue arrows the two closest peaks, one points to the left and the other to the right, but both correspond to a positive group velocity. They correspond to waves with a positive group velocity (energy is radiated away from the source) that match Snell's criteria on the interface (conservation of the parallel component of the wavevector). To illustrate Snell's law in this situation, we draw in figure S7(d) (resp. (e)) the spatial spectra corresponding to a homogeneous material (resp. square lattice). The wavenumber in the y direction has to be equal on both sides, which means the y component of the wave vector is the same in both cases, as illustrated by the dashed line in figures

S7(d)-(e). Waves can only propagate away from the source, so only waves corresponding to the right part of each circle can exist. This still leaves two possible wave vectors in the First Brillouin Zone, one pointing right and one pointing left, as illustrated in figure S7(e).

We can isolate each peak by filtering, and reconstruct the corresponding wave fields that we show in fig. S8(a-b). The peak with $k_x, k_y > 0$ corresponds to trivial positive refraction, while the peak with $k_x < 0, k_y > 0$ presents an apparent negative refraction. Movies showing how these 2 wave fields propagate are presented in Supplementary Information (Video 3). Note that this filtering allows to distinguish these two waves but that they cannot exist independently inside the crystal: because of the crystal's symmetry, they must co-exist.

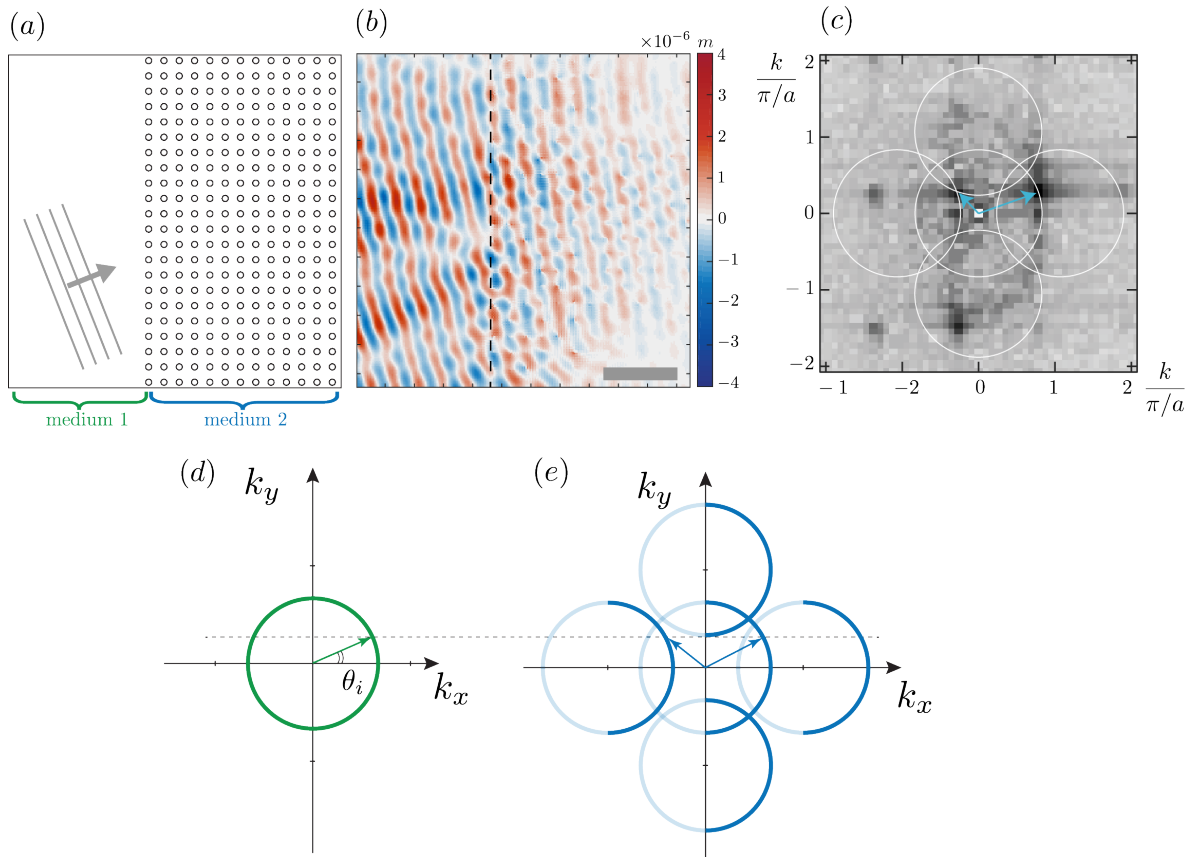

FIG. S7. (a) Sketch of the experiment showing the crystal of perforations and the incident plane wave. (b) Measured wave field (here filtered at the forcing frequency 60 Hz using a Fourier transform). (c) 2D spatial spectrum of the wave field inside the crystal. Information is represented in grayscale (darker means more signal) and in log scale. We add (in white) the circles corresponding to the theoretical dispersion relation, and we show with blue arrows the brightest peaks within the first Brillouin zone. (d) Isofrequency contour in a homoegeneous material. The green wave vector corresponds to the incident wave. (e) Isofrequency contour in a square lattice. Wave vectors that obey Snell's law are the intersection between the circles and the dashed line. We denote the two that are in the First Brillouin zone with blue arrows.

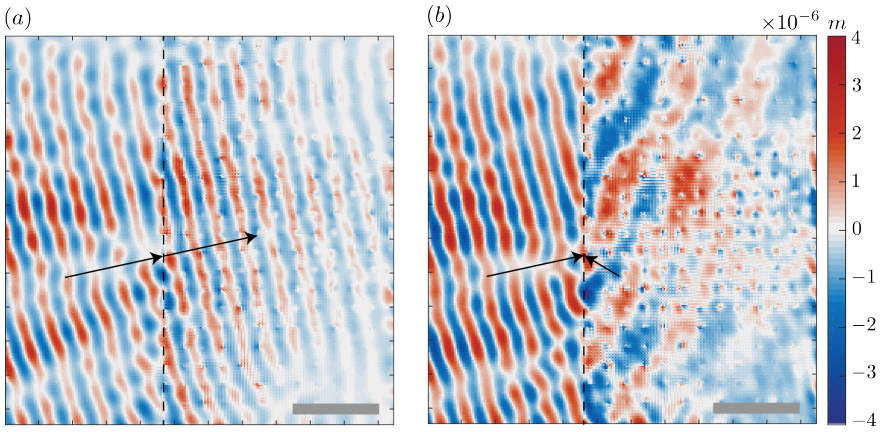

FIG. S8. Wave fields filtered and normalised to artificially isolate the two transmitted waves. The reconstructed wavefield (a) corresponds to the wave vector pointing right in fig. S7(c) while (b) corresponds to the one pointing left. The scale bar corresponds to 5 cm. See Supplementary Video 3.

VII. SUPPLEMENTARY VIDEOS

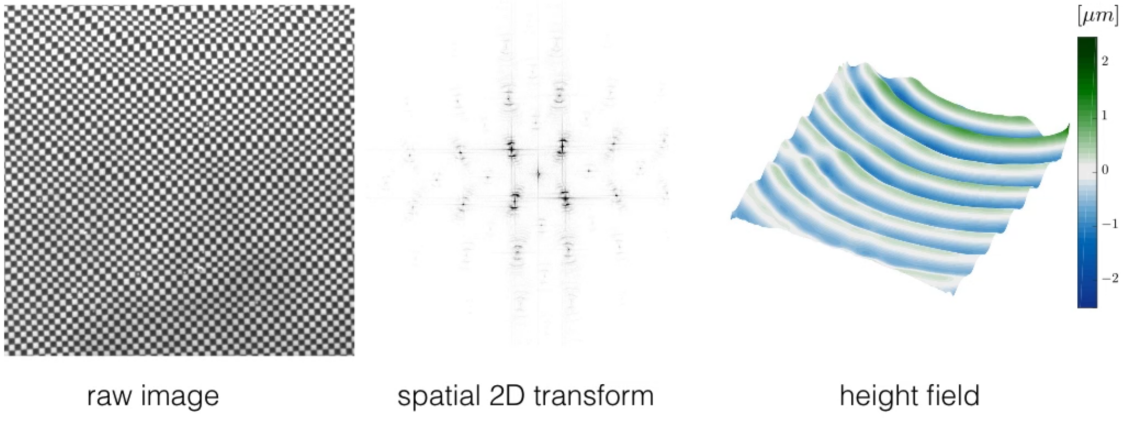

FIG. S9. View from Supplementary video 5 (Multimedia view).

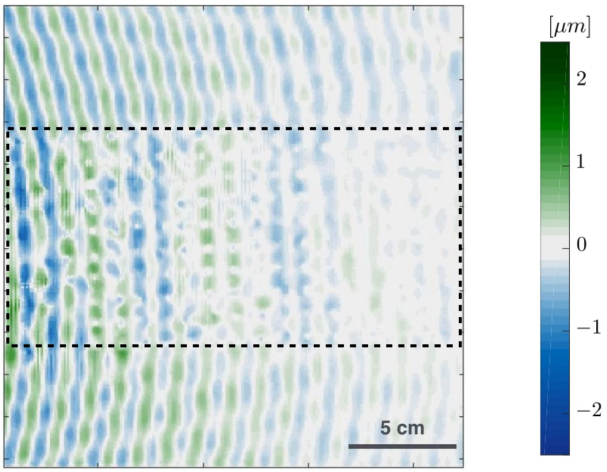

FIG. S10. View from Supplementary video 6 (Multimedia view).

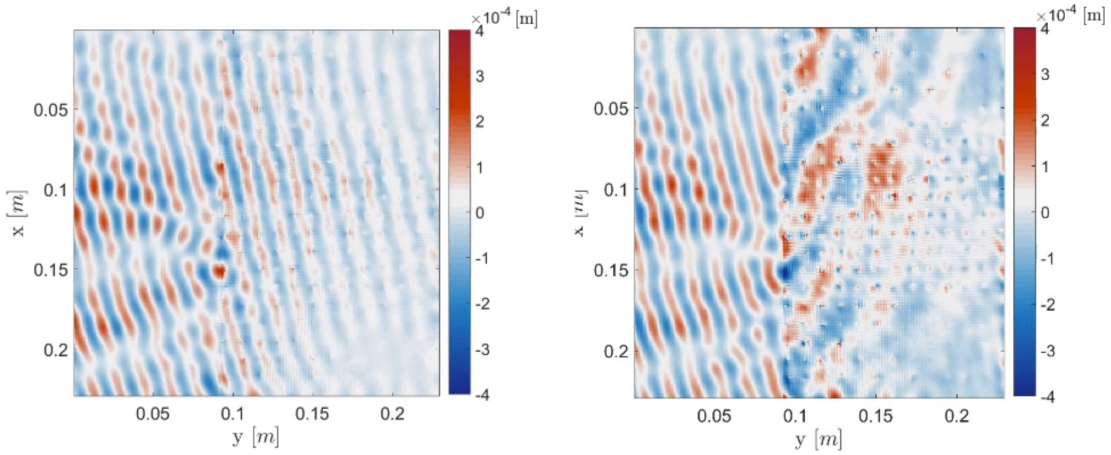

FIG. S11. View from Supplementary video 7 (Multimedia view).

[1] Ruben Manuel Sylvester Maria Schulkes, RJ Hosking, and AD Sneyd. Waves due to a steadily moving source on a floating ice plate. part 2. *Journal of Fluid Mechanics*, 180:297–318, 1987.

[2] JW Davys, RJ Hosking, and AD Sneyd. Waves due to a steadily moving source on a floating ice plate. *Journal of Fluid Mechanics*, 158:269–287, 1985.

[3] Lucie Domino, Marc Fermigier, Emmanuel Fort, and Antonin Eddi. Dispersion-free control of hydroelastic waves down to sub-wavelength scale. *EPL (Europhysics Letters)*, 121(1):14001, 2018.

[4] Frédéric Moisy, Marc Rabaud, and Kévin Salsac. A synthetic schlieren method for the measurement of the topography of a liquid interface. *Experiments in Fluids*, 46(6):1021–1036, Jan 2009.

[5] Sander Wildeman. Real-time quantitative schlieren imaging by fast fourier demodulation of a checkered backdrop. *Experiments in Fluids*, 59(6):97, May 2018.

[6] Here we present the Fast Checkerboard Demodulation (FCD) technique [5] but both work similarly.

[7] John D Joannopoulos, Steven G Johnson, Joshua N Winn, and Robert D Meade. *Photonic crystals: molding the flow of light*. Princeton university press, 2011.

[8] Fabrice Lemoult, Nadège Kaina, Mathias Fink, and Geoffroy Lerosey. Soda cans metamaterial: a subwavelength-scaled phononic crystal. *Crystals*, 6(7):82, 2016.

[9] Fabrice Lemoult, Nadege Kaina, Mathias Fink, and Geoffroy Lerosey. Wave propagation control at the deep subwavelength scale in metamaterials. *Nature Physics*, 9(1):55–60, 2013.

[10] Nadège Kaina. *Métamatériaux localement résonants: cristaux photoniques et phononiques sub-longueur d'onde*. PhD thesis, Université Paris 7, 2016.

[11] Nadege Kaina, Mathias Fink, and Geoffroy Lerosey. Composite media mixing bragg and local resonances for highly attenuating and broad bandgaps. *Scientific reports*, 3:3240, 2013.

[12] Pedro de Vries, David V. van Coevorden, and Ad Lagendijk. Point scatterers for classical waves. *Rev. Mod. Phys.*, 70:447–466, Apr 1998.